

Energy dependence of jet transport parameter and parton saturation in quark-gluon plasma

Jorge Casalderrey-Solana and Xin-Nian Wang

Nuclear Science Division, MS 70R0319, Lawrence Berkeley National Laboratory, Berkeley, CA 94720

(Dated: October 22, 2018)

We study the evolution and saturation of the gluon distribution function in the quark-gluon plasma as probed by a propagating parton and its effect on the computation of jet quenching or transport parameter \hat{q} . For thermal partons, the saturation scale Q_s^2 is found to be proportional to the Debye screening mass μ_D^2 . For hard probes, evolution at small $x = Q_s^2/6ET$ leads to jet energy dependence of \hat{q} . We study this dependence for both a conformal gauge theory in weak and strong coupling limit and for (pure gluon) QCD. The energy dependence can be used to extract the shear viscosity η of the medium since η can be related to the transport parameter for thermal partons in a transport description. We also derive upper bounds on the transport parameter for both energetic and thermal partons. The latter leads to a lower bound on shear viscosity-to-entropy density ratio which is consistent with the conjectured lower bound $\eta/s \geq 1/4\pi$. We also discuss the implications on the study of jet quenching at the BNL Relativistic Heavy Ion Collider and the CERN Large Hadron Collider and the bulk properties of the dense matter.

I. INTRODUCTION

Experimental data from the Relativistic Heavy-ion Collider (RHIC) have shown significant suppression of both high transverse momentum single inclusive hadron spectra and back-to-back dihadron correlation in central high-energy heavy-ion collisions [1, 2, 3]. The observed jet quenching phenomena can be attributed to parton energy loss and medium modification of the effective parton fragmentation functions [4, 5, 6] due to gluon bremsstrahlung induced by multiple parton scattering.

Within the picture of multiple parton scattering in QCD, the energy loss for an energetic parton propagating in a dense medium is dominated by induced gluon bremsstrahlung. Taking into account of the non-Abelian Landau-Pomeranchuk-Midgal (LPM) interference, the radiative parton energy loss [7],

$$\Delta E = \frac{\alpha_s N_c}{4} \hat{q}_R L^2, \quad (1)$$

is found to depend quadratically on the medium length L and a jet transport or energy loss parameter,

$$\hat{q}_R = \rho \int dq_T^2 \frac{d\sigma_R}{dq_T^2} q_T^2, \quad (2)$$

which describes the averaged transverse momentum transfer squared per unit distance (or mean-free-path). Here R is the color representation of the propagating parton in $SU(3)$ and ρ is the color charge density of the medium. According to this picture, jet quenching as observed in high-energy heavy-ion collisions is a direct measurement of the jet transport parameter \hat{q}_R in dense medium which not only characterizes the color charge density but also the interaction strength between the propagating parton and the medium.

Phenomenological studies based on variations of the parton energy loss picture [8, 9, 10, 11] all indicate the formation of an extremely high density matter in the

initial stage of high-energy heavy-ion collisions at the RHIC energy. The averaged transport parameter extracted from different phenomenological studies of the single inclusive high p_T hadron suppression in the most central $Au + Au$ collisions at RHIC is [12] $\hat{q}_F \sim 1 - 15$ GeV^2/fm (for a propagating quark) at an initial time $\tau_0 = 1$ fm/c . A recent simultaneous fit of the next-to-leading order (NLO) pQCD calculation to both single and back-to-back dihadron suppression [13] narrows the uncertainty to $\hat{q}_F = 1.1 - 1.4$ GeV^2/fm , which is still about 100 times higher than that in a cold nucleus $\hat{q}_F \approx 0.013$ GeV^2/fm as extracted from leading hadron suppression in deeply inelastic scattering off large nuclei [14].

In most of the theoretical studies of parton energy loss [7, 15, 16, 17, 18], except the twist-expansion approach [19], a static potential model for jet interaction with the medium was assumed which led to the factorized dependence of parton energy loss on the transport parameter \hat{q}_R in Eq. (1). In this static potential model, energy and longitudinal momentum transfer between a jet parton and the medium is ignored. Therefore, elastic energy loss due to the recoil of the medium parton during the jet-medium interaction is neglected in the calculation of radiative parton energy loss. Furthermore, the static potential model does not include the effect of inelastic break-up (or parton radiation) of the medium partons which can give rise to jet energy dependence of the transport parameter \hat{q}_R . In a dynamical picture, the transport parameter can be related to gluon distribution density of the medium [7]. The jet energy dependence of the transport parameter is then directly related to the scale and momentum fraction dependence of the gluon distribution density. Understanding the jet energy dependence of the transport parameter not only helps us to improve the phenomenological study of experimental data on jet quenching but also provides additional information about the structure of the dense quark-gluon matter in heavy-ion collisions. Furthermore, as illustrated in

a recent study [20], the low energy limit ($E \sim T$ temperature of the medium) of the transport parameter in jet quenching is directly related to the shear viscosity of the quark-gluon matter in a transport description. Therefore, experimental and theoretical study of the jet energy dependence of the transport parameter will be able to provide another piece of important information on bulk properties of the dense medium.

Recently, the transport parameter \hat{q}_R has also been calculated for a strongly coupled $\mathcal{N} = 4$ supersymmetric Yang-Mills (SYM) theory in different limiting scenarios. With a definition in terms of an adjoint Wilson loop along the light-cone, Liu, Rajagopal and Wiedemann [21] found that \hat{q}_A in the large limit of the t' Hooft coupling $\lambda = N_c g^2$ in SYM,

$$\hat{q}_A = \frac{\pi^{3/2} \Gamma(3/4)}{\Gamma(5/4)} \sqrt{\lambda} T^3, \quad (3)$$

scales with the temperature cubed and is independent of the jet (propagating parton) energy. In another limit for a slowly moving heavy quark, the transport parameter,

$$\hat{q}_F = 2\pi \sqrt{\lambda \gamma} T^3, \quad (4)$$

as defined in Eq. (2), is found [22, 23], to depend on the square-root of the heavy-quark energy, where $\gamma = E/M < (M/\sqrt{\lambda T})^2$. It is not clear how these two results are related to each other, though both describe the transport properties in a SYM theory.

In this paper, we investigate the jet energy dependence of the transport parameter \hat{q}_R within perturbative QCD (pQCD). We will first re-exam the relationship between the transport parameter and the unintegrated gluon distribution function of the color charges in the medium and how they are related to parton energy loss in the medium. For energetic jet partons, there are large logarithms of both momentum scale and small momentum fraction. They allow us to take double logarithmic approximation (DLA) and resum gluon radiation of the target color charges to all orders. The initial condition to such a resummed evolution of the gluon distribution can be calculated perturbatively within pQCD at finite temperature with hard thermal loop (HTL) resummation. From such resummed gluon distribution one can further take into account gluon saturation and calculate the saturation scale self-consistently which will determine the transport parameter and its jet energy dependence.

II. PARTON ENERGY LOSS, GLUON DISTRIBUTION FUNCTION AND TRANSVERSE MOMENTUM BROADENING

Multiple parton scattering within the high-twist expansion framework [24] can go beyond the static potential model and include energy and longitudinal momentum transfer in the calculation of medium modified fragmentation functions. The total energy loss for a propagating

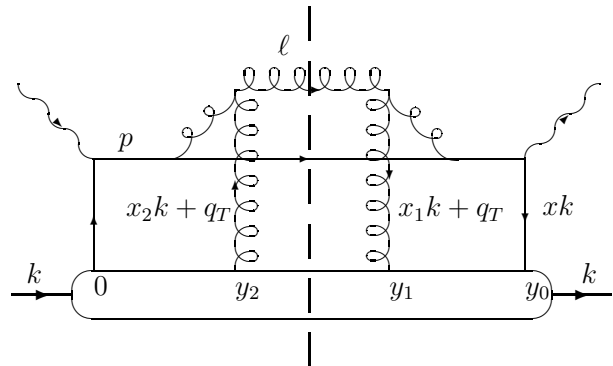


FIG. 1: Feynman diagram for induced gluon radiation that contributes to the quark energy loss.

parton in a deeply inelastic scattering (DIS) off a large nucleus as shown in Fig. 1 due to secondary quark-gluon scattering in this framework can be expressed as [19]

$$\frac{\Delta E}{E} = N_c \alpha_s \frac{2\alpha_s C_R}{N_c^2 - 1} \int \frac{d^2 q_T}{(2\pi)^2} \int d\ell_T^2 \int_0^1 dz \times \frac{1 + (1-z)^2 T_{qg}^A(x_B, x_L, q_T)}{\ell_T^2 (\ell_T^2 + \mu_T^2)} f_q^A(x_B), \quad (5)$$

where

$$x_L = \frac{\ell_T^2}{2z(1-z)p \cdot k}, \quad (6)$$

is the total longitudinal momentum transfer related to induced gluon radiation with final transverse momentum ℓ_T . A similar longitudinal momentum transfer

$$x_T = \frac{q_T^2 - 2\mathbf{q}_T \cdot \ell_T}{2(1-z)p \cdot k}, \quad (7)$$

is always provided by the initial gluon with transverse momentum q_T . As illustrated in Fig. 1, $p = [0, p^-, 0_T]$ is the initial quark momentum after its interaction with the photon, $k = [k^+, 0, 0_T]$ is the momentum per nucleon in the medium, q_T is the transverse momentum of the gluon exchange with the medium, ℓ_T is the transverse momentum and z is the fractional longitudinal momentum carried by the radiated gluon with four-momentum $\ell = [\ell_T^2/2zp^-, zp^-, \vec{\ell}_T]$. The quark distribution function $f_q^A(x_B)$ represents the production rate of the initial quark carrying x_B fraction of the nucleon longitudinal momentum in DIS. Eq. (5) is derived for quark energy loss and one can extend it for gluon by replacing the corresponding Casimir factor C_R for gluons. In the collinear expansion of the twist expansion approach, one normally makes Taylor expansion of the hard partonic parts in q_T and only the quadratic terms lead to the twist-four contribution. One can, however, approximate higher twist contributions from the q_T -dependence of the hard partonic part of the multiple scattering by using the average value $\langle q_T^2 \rangle = \mu_T^2$ in the cross section. As an extension

of the twist expansion, we will keep the integration over the gluon's transverse momentum q_T . The unintegrated quark-gluon correlation function is defined as,

$$\begin{aligned} T_{qg}^A(x, x_L, q_T) &= \int \frac{dy_0^-}{2\pi} dy_1^- dy_2^- d^2\xi_T e^{i(x+x_L)k^+ y_0^-} \\ &\times (1 - e^{-ix_L k^+ y_2^-})(1 - e^{-ix_L k^+ (y_0^- - y_1^-)}) \\ &\times e^{ix_T k^+ \xi^- - i\mathbf{q}_T \cdot \xi_T} \theta(-y_2^-) \theta(y_0^- - y_1^-) \\ &\times \langle A | \bar{\psi}_q(0) \frac{\gamma^+}{2} F_{\sigma^+}(y_2^-) F^{+\sigma}(y_1^-) \psi_q(y_0^-) | A \rangle, \end{aligned} \quad (8)$$

where $\xi = y_1 - y_2$, y_0 , y_1 and y_2 are space-time coordinates associated with the quark and gluon fields as illustrated in Fig. 1. The relative transverse coordinate ξ_T is the Fourier conjugate of the transverse momentum q_T in the gluon distribution function.

Even though the above parton energy loss is derived for quark production and propagation in DIS, it is also valid for high-energy heavy-ion collisions. In the latter case, we assume the life-time of the quark-gluon plasma to be much longer than its formation time and expansion time scale and therefore can treat thermal partons inside the produced dense matter as in asymptotic states. One therefore can neglect correlation between the initial production rate of the jet parton and the quark and gluon density of the produced medium. The quark-gluon correlation function will then take a factorized form,

$$\begin{aligned} \frac{T_{qg}^A(x, x_L, q_T)}{f_q^A(x)} &= \int dy^- \int \frac{d^3k}{(2\pi)^3 2k^+} f(k, y) d\xi^- d^2\xi_T \\ &\times e^{ix_T k^+ \xi^- - i\mathbf{q}_T \cdot \xi_T} (k | F_{\sigma^+}(y_2^-) F^{+\sigma}(y_1^-) | k) \\ &\times \left[e^{ix_L k^+ \xi^-} (1 - e^{ix_L k^+ y^-}) + c(x_L) (1 - e^{-ix_L k^+ y^-}) \right] \\ &= \pi \int dy^- \int \frac{d^3k}{(2\pi)^3} f(k, y) [1 - \cos(x_L k^+ y^-)] \\ &\times [\phi_k(x_T + x_L, q_T) + c(x_L) \phi_k(x_T, q_T)], \end{aligned} \quad (9)$$

where $f(k, y)$ is the local phase space distribution of the color sources in the medium and $c(x_L) = f_q(x + x_L)/f_q(x)$ is the relative initial quark distributions in DIS and is given by the corresponding ratio of jet production cross sections in heavy-ion collisions. The unintegrated gluon distribution function per color source $\phi_k(x, q_T)$ is defined as

$$\begin{aligned} \phi_k(x, q_T) &= \int \frac{d\xi^-}{2\pi k^+} d^2\xi_T e^{ix k^+ \xi^- - i\mathbf{q}_T \cdot \xi_T} \\ &\times \langle k | F^{\sigma^+}(0) F_{\sigma^+}^+(\xi^-, \xi_T) | k \rangle. \end{aligned} \quad (10)$$

The structure of the quark-gluon correlation function in Eq. (9) corresponds to two different bremsstrahlung processes and their interference [19] associated with the different pole structures in Fig. 1. One can also categorize them according to how the longitudinal momentum transfer x_L is provided. In the first term, the final gluon is induced by the secondary scattering with the medium gluon in which the intermediate gluon is off-shell. The longitudinal momentum transfer x_L is therefore provided

by the medium gluon and the contribution is proportional to gluon distribution $\phi_k(x_T + x_L, q_T)$ per medium or ‘‘constituent’’ parton. These secondary processes correspond to quark-gluon Compton scattering where the initial gluon comes from a thermal constituent parton with a gluon distribution $\phi_k(x_T + x_L, q_T)$. Among these processes, one can identify a special case in which the quark scatters directly with a medium constituent gluon ($x_L = 1$) as purely elastic processes and the corresponding energy loss as the conventional elastic energy loss [25]. The second term in Eq. (9) corresponds to the processes in which gluon radiation is induced by the hard scattering that produces the initial jet (the quark after the photon interaction in Fig. 1 is off-shell) and the final gluon scatters again with a soft medium gluon with momentum fraction x_T . It is therefore proportional to the soft gluon distribution $\phi_k(x_T, q_T)$. The longitudinal momentum transfer x_L of the bremsstrahlung in this case is provided by the initial hard process with the cross section given in $c(x_L)$.

One can now define a generalized jet transport parameter,

$$\begin{aligned} \hat{q}_R(E, x_L, y) &= \frac{4\pi^2 \alpha_s C_R}{N_c^2 - 1} \int \frac{d^3k}{(2\pi)^3} f(k, y) \\ &\times \int \frac{d^2q_T}{(2\pi)^2} \phi_k(x_T + x_L, q_T), \end{aligned} \quad (11)$$

which includes the extra longitudinal momentum transfer x_L from the medium to the propagating parton and the radiated gluon. The total parton energy loss from Eq. (5) can be expressed as

$$\begin{aligned} \frac{\Delta E}{E} &= \frac{\alpha_s N_c}{\pi} \int dy^- dz d\ell_{\perp}^2 \frac{1 + (1 - z)^2}{\ell_T^2 (\ell_T^2 + \mu_T^2)} [\hat{q}_R(E, x_L, y) \\ &+ c(x_L) \hat{q}_R(E, 0, y)] \sin^2 \left[\frac{\ell_T^2 y^-}{4Ez(1 - z)} \right], \end{aligned} \quad (12)$$

in terms of the generalized jet transport parameter. The first term with the generalized transport parameter involves energy transfer between the propagating parton and the medium. It contains (but not limited to) what is normally defined as pure elastic energy loss [25]. The second term that is proportional to the normal (or special) transport parameter $\hat{q}_R(E, y) = \hat{q}_R(E, x_L = 0, y)$ corresponds to pure radiative energy loss.

Completing the integration over the phase-space of the radiated gluon, one can recover from the second term a similar form of total radiative energy loss in a static and uniform medium with finite length as in Eq. (1). However, one needs to know the x_L -dependence of the unintegrated gluon distribution function in order to calculate the ‘‘elastic’’ part of the energy loss. Furthermore, the transport parameter as defined in Eq. (2) should have some non-trivial jet energy (E) and temperature (T) dependence.

Within the framework of twist expansion, the transverse momentum broadening of the quark jet has also

been calculated [26],

$$\langle \Delta p_T^2 \rangle = \frac{4\pi\alpha_s C_R}{N_c^2 - 1} \frac{T_{qg}^A(x, 0)}{f_q^A(x)} = \int dy^- \hat{q}_R(E, 0, y), \quad (13)$$

which is directly related to the normal transport parameter $q_R(E, y) \equiv q_R(E, 0, y)$ as defined in Eq. (11) in terms of the unintegrated gluon distribution density of the medium. The jet transport parameter $q_R(E, y)$ therefore can be interpreted as the transverse momentum broadening per unit length for the propagating parton, as defined in Eq. (2). Resummation of higher twist contributions leads to a diffusion equation for the transverse momentum distribution in which the above is the averaged transverse momentum broadening [27].

The approach leading to the above total energy loss and transverse momentum broadening has gone beyond the conventional static potential model in two aspects: (a) The result includes the longitudinal momentum transfer (x_T) between the jet parton and the medium parton, which is related to the transverse momentum transfer (q_T) through the unintegrated gluon distribution density of the medium. This will result in the jet energy dependence of both the generalized and the normal transport parameter $\hat{q}_R(E, y)$ (or transverse momentum broadening) which is absent in the static potential model. (b) The formula also includes the processes in which longitudinal momentum transfers x_L comes from the medium parton and therefore it depends on the generalized jet transport parameter $\hat{q}_R(x_L)$. It contains contributions from elastic energy loss.

For the remainder of this paper we will focus on the energy dependence of the normal transport parameter $\hat{q}_R \equiv \hat{q}_R(E, y)$. Since it is essentially the transverse momentum broadening per unit length which can be directly measured in experiments such as DIS and γ -jet events in heavy-ion collisions, we will suppress the space and time dependence to simplify the notation.

III. GLUON DISTRIBUTION IN A QUARK-GLUON PLASMA

As shown in Eq. (11), the transport parameter \hat{q}_R experienced by a propagating parton can be defined in terms of the unintegrated gluon distributions $\phi_k(x, q_T^2)$ of the color sources in the quark-gluon plasma. After averaging over the momentum of the color sources, it can be expressed as,

$$\hat{q}_R = \frac{4\pi^2 C_R}{N_c^2 - 1} \rho \int_0^{\mu^2} \frac{d^2 q_T}{(2\pi)^2} \int dx \times \delta(x - \frac{q_T^2}{2p^- \langle k^+ \rangle}) \alpha_s \langle q_T^2 \rangle \phi(x, q_T^2), \quad (14)$$

where $\langle k^+ \rangle$ is the average energy of the color sources and $\phi(x, q_T^2)$ is the corresponding average unintegrated gluon

distribution function per color source. The integrated gluon distribution is

$$xG(x, \mu^2) = \int_0^{\mu^2} \frac{d^2 q_T}{(2\pi)^2} \phi(x, q_T). \quad (15)$$

We have extended our earlier definition of \hat{q}_R to include the case of a running strong coupling constant α_s in QCD. We will refer to the case of fixed coupling constant as conformal gauge theory. However, for any scale below the temperature $\mu^2 \leq T^2$ we will consider α_s frozen and treat it as a constant.

Consider the lowest order parton-parton small angle scattering, we can obtain \hat{q}_R as,

$$\hat{q}_R = \sum_b \nu_b g^4 C_{Rb} \int \frac{d^3 k}{(2\pi)^3} f_b(k) (1 \pm f_b(k')) q_T^2 |\mathcal{M}_{Rb}|^2 \times \frac{d^3 k'}{(2\pi)^3} \frac{d^3 p'}{(2\pi)^3} (2\pi)^4 \delta^4(p + k - p' - k'), \quad (16)$$

where \mathcal{M}_{Rb} is the truncated parton-parton scattering matrix element,

$$\mathcal{M}_{Rb} \approx \left[\frac{1}{q^2 + \mu_D^2 \pi_L(x_q)} - \frac{(1 - x_q^2) \cos \phi}{q^2(1 - x_q^2) + \mu_D^2 \pi_T(x_q) + \mu_{\text{mag}}^2} \right], \quad (17)$$

where $\cos \phi = (\vec{v} \times \vec{q}) \cdot (\vec{v}_b \times \vec{q}) / q^2$, $x_q = q_0 / q$ and $\mu_D^2 = g^2(N_c + n_f/2)T^2/3$ is the Debye screening mass in thermal QCD medium with temperature T and $\mu_{\text{mag}} \approx N_c g^2 / 2\pi$ is the non-perturbative magnetic screening mass [28, 29, 30]. The color factors for different scatterings are $C_{qq} = C_F / 2N_c$, $C_{qg} = 1/2$, $C_{gg} = N_c^2 / (N_c^2 - 1)$. The statistical factor ν_b is $2(N_c^2 - 1)$ for gluons and $4N_c n_f$ for n_f flavors of quarks. We use an effective gluon propagator to include the resummation of hard thermal loops (HTL) [31]. The scaled self-energies in the effective propagator in the long-wavelength limit are given by [32],

$$\begin{aligned} \pi_L(x_q) &= 1 - \frac{x_q}{2} \ln \left(\frac{1 + x_q}{1 - x_q} \right) + i \frac{\pi}{2} x_q, \\ \pi_T(x_q) &= \frac{x_q^2}{2} + \frac{x_q}{4} (1 - x_q^2) \ln \left(\frac{1 + x_q}{1 - x_q} \right) \\ &\quad - i \frac{\pi}{4} x_q (1 - x_q^2). \end{aligned} \quad (18)$$

One can rewrite the phase-space integration in Eq (16) as

$$\begin{aligned} &\int \frac{d^3 k'}{(2\pi)^3} \frac{d^3 p'}{(2\pi)^3} (2\pi)^4 \delta^4(p + k - p' - k') \\ &= \frac{1}{(2\pi)^2} \int dx d^2 q_T \delta(x - \frac{q_T^2}{2p^- k^+}), \end{aligned} \quad (20)$$

where $x = q^+ / k^+$. For small angle scattering, one can set $q^2 \approx q_T^2$ and $x_q \approx x k^+ / q_T$. We further approximate

k^+ by its average value $\langle k^+ \rangle = 3T$ in the scattering matrix. Note that energy-momentum conservation fixes the relative angle between k and q . Therefore, the angular phase-space for k is only 2π . One can complete the rest of the phase-space integration over the initial momentum,

$$\begin{aligned} \int \frac{k^2 dk}{4\pi^2} f_b(k)(1 \pm f_b(k')) &\approx \int \frac{k^2 dk}{4\pi^2} f_b(k)(1 \pm f_b(k)) \\ &= \frac{T^3}{12} \text{ (gluons)} \text{ or } \frac{T^3}{24} \text{ (quarks)}. \end{aligned} \quad (21)$$

Using

$$\frac{1}{2}C_{Rq}\nu_q + C_{Rg}\nu_g = 2N_c C_R \left(1 + \frac{n_f}{2N_c}\right), \quad (22)$$

and

$$\rho = \frac{T^3}{\pi^2} \zeta(3) \left(\nu_g + \frac{3\nu_q}{4}\right) = 2(N_c^2 - 1) \left(1 + \frac{3n_f}{4C_F}\right) \frac{T^3}{\pi^2} \zeta(3), \quad (23)$$

one can express Eq. (16) as

$$\begin{aligned} \hat{q}_R &= \frac{4\pi^2 \alpha_s C_R}{N_c^2 - 1} \rho N_c \frac{\alpha_s}{2\pi} \frac{\pi^2}{6\zeta(3)} \frac{1 + n_f/2N_c}{1 + 3n_f/4C_F} \\ &\times \int dx dq_T^2 \delta(x - \frac{q_T^2}{2p^-\langle k^+ \rangle}) q_T^2 |\mathcal{M}_{Rb}|^2. \end{aligned} \quad (24)$$

The factor $\pi^2/6\zeta(3)$ comes from the quantum statistics effect for the final state partons in the scattering processes. According to the definition in Eq. (14), one can obtain the unintegrated gluon distribution function,

$$\phi(x, q_T^2) = 2N_c \alpha_s \frac{\pi^2}{6\zeta(3)} \frac{1 + n_f/2N_c}{1 + 3n_f/4C_F} |\mathcal{M}_{Rb}|^2 q_T^2, \quad (25)$$

in a quark-gluon plasma and the integrated gluon distribution function is

$$\begin{aligned} xG(x, \mu^2) &= \frac{N_c \alpha_s}{2\pi} \frac{\pi^2}{6\zeta(3)} \frac{1 + n_f/2N_c}{1 + 3n_f/4C_F} \\ &\times \int_0^{\mu^2} dq_T^2 |\mathcal{M}_{Rb}|^2 q_T^2. \end{aligned} \quad (26)$$

We concentrate in the small x_q region, $x_q = 3xT/q_T \ll 1$. For a typical momentum transfer of the order of μ_D , the requirement that x_q is small leads to $x \ll (\sqrt{N_c}g^2/3)/3$. Within this approximation, we obtain

$$\pi_L(x_q) \approx 1 - ix \frac{3\pi T}{2q_T}, \quad \pi_T(x_q) \approx -ix \frac{3\pi T}{4q_T}, \quad (27)$$

and

$$\phi(x, q_T^2) = \frac{2N_c \alpha_s}{\mu_D^2} \frac{\pi^2}{6\zeta(3)} \frac{1 + n_f/2N_c}{1 + 3n_f/4C_F} \tilde{\phi}(x, y_q); \quad (28)$$

$$\begin{aligned} \tilde{\phi}(x, y_q) &\equiv \mu_D^2 |\mathcal{M}_{Rb}|^2 q_T^2 \\ &\approx \frac{y_q^2}{y_q(y_q + 1)^2 + x^2 9\pi^2 T^2 / 4\mu_D^2} \\ &+ \frac{1}{2} \frac{y_q^2}{y_q(y_q + \mu_{\text{mag}}^2/\mu_D^2)^2 + x^2 9\pi^2 T^2 / 16\mu_D^2}, \end{aligned} \quad (29)$$

where $y_q = q_T^2/\mu_D^2$. For $x \gg 4\mu_{\text{mag}}/\pi = 2N_c g^2/\pi^2$, one can neglect the magnetic mass and complete the integration in Eq. (26) and obtain

$$\begin{aligned} xG(x, \mu^2) &\approx N_c \frac{\alpha_s}{2\pi} \frac{\pi^2}{6\zeta(3)} \frac{1 + n_f/2N_c}{1 + 3n_f/4C_F} \\ &\times \left\{ \left[\ln\left(1 + \frac{\mu^2}{\mu_D^2}\right) - \frac{\mu^2/\mu_D^2}{1 + \mu^2/\mu_D^2} \right] \right. \\ &\times \left[1 - 0.035 \frac{3xT}{\mu_D} \right] e^{-3xT\mu_D/\mu^2} \\ &\left. + \frac{1}{6} \ln\left(1 + \frac{16}{9\pi^2} \frac{\mu^6}{x^2 T^2 \mu_D^4}\right) \right\}, \end{aligned} \quad (30)$$

where the first term is an approximation of the numerical integration from the electric part of the interaction for $x \leq 2\mu_D/3\pi T = 2\sqrt{N_c}g^2/3/3\pi$. Because of the static Debye screening, it has a very weak x dependence in this x region, which can be ignored for large values of $\mu/\mu_D \geq 1$. The magnetic part of interaction, on the other hand, has only dynamical screening and therefore lead to the dominant x dependence of the gluon distribution from a quark-gluon plasma at small x . However, our approximations are not valid for $x \leq 4\mu_{\text{mag}}/3\pi T \approx 2N_c g^2/3\pi^2$, where the non-perturbative magnetic mass [28, 29, 30] $\mu_{\text{mag}} \approx N_c g^2/2\pi$ becomes important. In this region, the logarithmic x -dependence of the gluon distribution from the magnetic interaction disappears and is replaced by a constant $\ln(\mu^2/\mu_{\text{mag}}^2)$.

For large $\mu^2/\mu_D^2 \gg 1$ in the small $N_c g^2 < x < \sqrt{N_c}g$ region of a pure gluonic plasma ($n_f = 0$), the gluon distribution per gluonic color source is then,

$$xG(x, \mu^2) \approx C_A \frac{\alpha_s}{\pi} \frac{\pi^2}{6\zeta(3)} \frac{1}{2} \left[\frac{3}{2} \ln \frac{\mu^2}{\mu_D^2} + \frac{1}{3} \ln \frac{\mu_D}{xT} \right], \quad (31)$$

which is generated from perturbative gluon radiation. For a pure quark plasma, the corresponding gluon distribution for each quark color source is

$$xG(x, \mu^2) \approx C_F \frac{\alpha_s}{\pi} \frac{\pi^2}{6\zeta(3)} \frac{1}{3} \left[\frac{3}{2} \ln \frac{\mu^2}{\mu_D^2} + \frac{1}{3} \ln \frac{\mu_D}{xT} \right]. \quad (32)$$

For the remainder of this paper, we will focus on a pure gluonic plasma.

IV. GLUON SATURATION IN A PLASMA

Similar to gluon saturation in a large nucleus at small x , saturation could also happen in the small x region of a quark-gluon plasma. The saturation scale is given by [33]

$$Q_s^2(x) = \frac{4\pi^2 N_c \alpha_s}{N_c^2 - 1} \rho xG(x, Q_s^2) \min(L, L_c) \quad (33)$$

where $L_c = 1/xT$ is the coherence length for parton scattering in a thermal medium. Since the HTL resummation does not include coherence effects, the use of the

gluon distribution in Eq. (31) requires that the mean-free-path of thermal gluons must be larger than the coherence length. Given the perturbative expression of the mean-free-path [20],

$$\lambda_f^{-1} = \langle \rho \sigma_{\text{tr}} \rangle \approx \frac{4\zeta(3)}{9\pi} N_c^2 \alpha_s^2 T \ln \frac{1}{N_c \alpha_s}, \quad (34)$$

this implies,

$$\frac{L_c}{\lambda_f} = \frac{4\zeta(3)}{9\pi} \frac{N_c^2 \alpha_s^2}{x} \ln \frac{1}{N_c \alpha_s} \leq 1, \quad (35)$$

or

$$x \geq \frac{4\zeta(3)}{9\pi} N_c^2 \alpha_s^2 \ln \frac{1}{N_c \alpha_s} \sim (N_c \alpha_s)^2 \ln \frac{1}{N_c \alpha_s}. \quad (36)$$

In this regime, one can use the perturbative gluon distribution [Eq. (31)] to determine the saturation scale,

$$\begin{aligned} Q_s^2(x) &= \frac{4\pi^2 N_c \alpha_s}{N_c^2 - 1} \rho x G(x, Q_s^2) L_c \\ &= \frac{\pi}{x} (N_c \alpha_s)^2 T^2 \left[\ln \frac{Q_s^2}{\mu_D^2} + \frac{2}{9} \ln \frac{\mu_D}{xT} \right]. \end{aligned} \quad (37)$$

Neglecting the logarithmic terms, one can get a simple expression for the saturation scale in the perturbative regime,

$$Q_s^2(x)/T^2 \sim \frac{(N_c g^2)^2}{x}. \quad (38)$$

Since $\mu_D^2 = N_c g^2 T^2/3 \sim N_c g^2 T^2$, we note the following hierarchy of the saturation scale in a perturbative gluonic plasma

$$\begin{aligned} Q_s^2(x) &\sim (N_c g^2)^2 T^2 \sim \mu_{\text{mag}}^2, \text{ for } x \sim 1 \\ Q_s^2(x) &\sim N_c g^2 T^2 \sim \mu_D^2, \text{ for } x \sim N_c g^2 \sim \frac{\mu_D^2}{T^2} \\ Q_s^2(x) &\sim T^2, \text{ for } x \sim N_c^2 g^4 \sim \frac{\mu_{\text{mag}}^2}{T^2}, \end{aligned} \quad (39)$$

as illustrated in Fig. 2.

In the calculation of \hat{q}_R for interaction among thermal partons, the typical $x_m = Q_s^2/\langle \hat{s} \rangle = Q_s^2/18T^2$. One can determine the saturation scale at x_m from Eq. (37)¹,

$$Q_s^2(x_m) \approx \mu_D^2 \frac{3}{2} \sqrt{\frac{1}{\pi} \ln \frac{18T}{\mu_D}}. \quad (40)$$

It is interesting to note that the gluon saturation scale for interaction among thermal partons coincides approximately with the Debye screening mass. Therefore, resummation of HTL effectively provides some kind of mechanism for gluon saturation in a thermal gluon plasma.

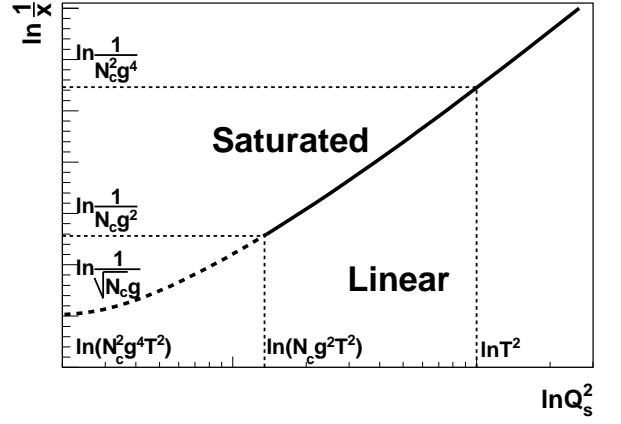


FIG. 2: Illustration of the hierarchy of the saturation scale $Q_s^2(x)$ below the hard scale $\mu^2 = T^2$ in a weak coupling gluonic plasma.

To obtain the transport parameter \hat{q}_R at scale $\mu^2 \leq T^2$ due to interaction with the gluonic color sources via exchange of HTL gluons, one has to complete the integral in Eq. (24). A simple integration in Eq. (24) without considering effect of gluon saturation gives

$$\hat{q}_R \approx \frac{14}{15} \pi N_c^2 \alpha_s^2 T^3 \ln \frac{\mu^2}{\mu_D^2}, \quad (41)$$

as obtained by a previous calculation of \hat{q}_R with dynamic screening [34]. One can also obtain the above result from the integrated gluon distribution

$$\hat{q}_R \simeq \frac{4\pi^2 C_R}{N_c^2 - 1} \rho [xG(x, \mu^2)]_{x=\mu_D^2/\mu^2}. \quad (42)$$

In principle, one should take into account the effect of gluon saturation in evaluating the transport parameter in the region $q_T^2 < Q_s^2(x)$. In this regime, we can follow KNL model [35] and assume the saturated unintegrated gluon distribution as a constant in q_T ,

$$\phi(x, q_T^2) = \frac{2N_c \alpha_s}{\mu_D^2} \frac{\pi^2}{6\zeta(3)} \begin{cases} \tilde{\phi}(x, Q_s^2/\mu_D^2), & q_T^2 < Q_s^2; \\ \tilde{\phi}(x, q_T^2/\mu_D^2), & q_T^2 > Q_s^2, \end{cases} \quad (43)$$

where $\tilde{\phi}(x, y_q)$ is given by Eq. (29) and the saturation scale $Q_s^2(x)$ is determined by Eq. (37). Using the above model for gluon distribution in the saturated regime in Eq. (14), one can evaluate the thermal parton transport parameter. The result,

$$\hat{q}_R \approx \pi N_c^2 \alpha_s^2 T^3 \ln \frac{Q_m^2}{\mu_D^2}, \quad (44)$$

with $Q_m^2 = 18T^2$, is nearly identical to Eq. (41). This is because the dominant contribution to the parton transport parameter comes from $q_T^2 > Q_s^2$ for large $Q_m^2/\mu_D^2 >$

¹ Note that the typical $x_m \sim N_c g^2$; thus the breakdown of the approximation in Eq. (31) due to magnetic mass coincides with the onset of non-linear effects

1 and therefore the effect of gluon saturation is negligible in the calculation of transport parameter for thermal partons.

The similarity between results in Eqs. (44) and (41) is also an indication that saturation effect is already present in the unintegrated gluon distribution function $\phi(x, q_T^2)$ in Eqs. (28) and (29) due to HTL resummation. One can clearly see this by analyzing the unintegrated gluon distribution $\phi(x, q_T^2)$ [Eqs. (28) and (29)] at $x = q_T^2/\langle\hat{s}\rangle$. For large $q_T^2 \gg \mu_D^2$, $\phi(x, q_T^2) \sim 1/q_T^2$. The electric contribution to $\phi(x, q_T^2)(x = q_T^2/\langle\hat{s}\rangle)$ reaches its peak value $\sim N_c\alpha_s/\mu_D^2$ at $q_T^2 \approx \mu_D^2 \sim Q_s^2$ and vanishes at $q_T^2 = 0$. Without the magnetic mass, the magnetic contribution to $\phi(x, q_T^2)(x = q_T^2/\langle\hat{s}\rangle)$, however, continues to increase at $q_T^2 < Q_s^2 \sim \mu_D^2$ and reaches a finite value $\phi(x, q_T^2)(x = q_T^2/\langle\hat{s}\rangle) \sim 1/\mu_D^2$ at $q_T^2 \ll \mu_D^4/T^2$. However, contribution to \hat{q}_R from this region of limited phase space is sub-leading in the leading logarithmic approximation.

V. EVOLUTION OF THE THERMAL GLUON DISTRIBUTION

The gluon distribution function in Eq. (31) was obtained via parton interaction in a thermal medium with a HTL resummed gluon propagator and, thus, is only valid for scales $\mu^2 < T^2$. At larger scales, radiation of hard modes, *i.e.*, partons with momentum $k > T$, is possible. These processes lead to the evolution of the gluon distribution which in vacuum is governed by the BFKL/DGLAP equations in the linearized regime. In the medium this evolution may be modified due to the interaction of the radiated gluons with thermal partons. However, since the medium effects are of the order of $\mu_D \ll T$, we neglect those at hard scales and use the vacuum evolution to determine the gluon distribution. The previous computation in Eq. (31) serves as an initial condition of this evolution at $\mu^2 = T^2$.

Since we are interested in the determination of \hat{q}_R at large jet energies, we need to know the unintegrated parton distribution $\phi(x, q_T^2)$ in Eq. (14) at small $x \sim \langle q_T^2 \rangle / 6ET$. For a large path length, the typical total momentum transfer, $\hat{q}L$, which will set the scale of the process, is also large. This is the regime of the double logarithmic approximation (DLA), in which the BFKL and DGLAP equations coincide [36, 37]. In this approximation, all terms enhanced by two large logarithms of the type

$$\left(\alpha_s(k^2) N_c \ln \frac{k^2}{\mu^2} \ln \frac{1}{x} \right)^n, \quad (45)$$

are resummed. Thus, the DLA approximation is valid if terms of the above type are larger than those of type

$$\left(\alpha_s(k^2) N_c \ln \frac{1}{x} \right)^n, \quad \left(\alpha_s(k^2) N_c \ln \frac{k^2}{\mu^2} \right)^n. \quad (46)$$

The resummation of the terms in Eq. (45) leads to the

evolution equation,

$$\frac{\partial^2 xG(y, \xi)}{\partial y \partial \xi} = \frac{1}{2} xG(y, \xi), \quad (47)$$

where, following Ref. [36], we have defined variables y and ξ as ²

$$\xi = \int_{\mu^2}^{Q^2} \frac{dk^2}{k^2} \frac{2\alpha_s(k)N_c}{\pi}, \quad (48)$$

$$y = \ln \frac{1}{x}. \quad (49)$$

The asymptotic solution to Eq. (47) leads to a growth of the gluon distribution function of the order $\exp(\sqrt{2\xi y})$, while resummation of terms in Eq. (46) leads to $\exp(\alpha_s N_c y)$ and $\exp(\xi)$ respectively [36]. Therefore, the DLA approximation is valid as long as

$$\xi \ll \sqrt{\xi y}, \quad (50)$$

$$\alpha N_c y \ll \sqrt{\xi y}. \quad (51)$$

Note that the definition of ξ allows to describe simultaneously the evolution of a conformal and non-conformal theory. For these two cases we have

$$\xi(Q^2) = \begin{cases} \bar{\lambda} \ln(Q^2/\mu^2) & \text{for fixed } \alpha_s \\ \frac{2N_c}{\pi b} \ln \frac{\ln(Q^2/\Lambda^2)}{\ln(\mu^2/\Lambda^2)} & \text{for running } \alpha_s \end{cases} \quad (52)$$

where the reduced t'Hooft coupling is $\bar{\lambda} = 2N_c\alpha_s/\pi$ and $b = (11N_c - 2N_f)/12\pi$.

The general solution of Eq. (47) can be found by performing a Laplace transformation and is given by [37, 38]

$$xG(x, Q^2) = \int_{a-i\infty}^{a+i\infty} \frac{dn}{2\pi i} e^{ny + \frac{\xi}{2n}} D(n), \quad (53)$$

where a is any real number larger than the real part of any poles of $D(n)$. The corresponding Laplace transformation $D(n)$ of the gluon distribution in Eq. (31) at $Q^2 = \mu^2 = T^2$ ($\xi = 0$) is:

$$\begin{aligned} D(n) &= \int_{0^-}^{\infty} dy e^{-ny} xG(x, T^2) \\ &= \frac{N_c\alpha_s^T}{2\pi} \frac{\pi^2}{6\zeta(3)} \frac{1}{3} \left[\frac{1}{n} 4 \ln \frac{T^2}{\mu_D^2} + \frac{1}{n^2} \right], \end{aligned} \quad (54)$$

where α_s^T is the strong coupling constant α_s evaluated at a scale that is proportional to T^2 , since Eq. (31) is obtained through scattering between thermal partons.

² The definition we use is slightly different from that of [36] and is more suitable for the description of a conformal plasma (α_s fixed)

For large $y\xi$ values, the integral in Eq. (53) can be performed by saddle point approximation, yielding

$$xG(x, Q^2) = \frac{N_c \alpha_s^T}{2\pi} \frac{\pi^2}{6\zeta(3)} \frac{1}{3} \frac{e^{\sqrt{2\xi y}}}{\sqrt{\pi}(2\xi y)^{1/4}} \times \left[2 \ln \frac{T^2}{\mu_D^2} + \frac{y}{(2\xi y)^{1/2}} \right]. \quad (55)$$

The above evolved gluon distribution function grows rapidly (faster than a power) with the rapidity y . Thus, at large y non-linear effects become important leading to parton saturation. Similarly, we can determine the saturation scale $Q_s^2(x)$ from Eq. (33) with the above gluon distribution function $xG(x, Q)$,

$$Q_s^2 = B(x, Q_s^2) \min(L, L_c) \exp \left\{ \sqrt{2\xi_s y} \right\}, \quad (56)$$

where $\xi_s = \xi(Q_s^2)$ and

$$B(x, Q_s^2) = \frac{1}{9} \frac{\pi^3}{\zeta(3)} \frac{N_c \alpha_s(Q_s^2)}{N_c^2 - 1} \rho \frac{N_c \alpha_s^T}{\sqrt{\pi}(2\xi_s y)^{1/4}} \times \left[2 \ln \frac{T^2}{\mu_D^2} + \frac{y}{(2\xi_s y)^{1/2}} \right]. \quad (57)$$

In solving the self-consistent equation Eq. (56) we will neglect the weak dependence of $B(x, Q_s)$ on x and ξ_s and treat it as a constant as compared to the dependence in the exponent. This is an approximation we will take throughout this paper.

We now can use the evolved gluon distribution function in Eq. (55) to compute the jet transport parameter as defined in Eq. (14). In the linear evolution region ($q_T^2 > Q_s^2$), the unintegrated parton distribution is computed by taking the derivative of Eq. (55) with respect to the scale. Keeping the leading term in ξy (*i.e.* consider only the ξy dependence in the exponent) we find

$$\begin{aligned} \phi_{DLA}(x, q_T^2) &= 4\pi \frac{\partial}{\partial q_T^2} xG(x, q_T^2) \\ &\approx 8 \frac{y}{\sqrt{2\xi y}} \frac{\alpha_s(q_T^2) N_c}{q_T^2} xG(x, q_T^2). \end{aligned} \quad (58)$$

Using Eq. (33), we find at $q_T^2 = Q_s^2$,

$$\phi_{DLA}(x, Q_s^2) = \frac{2}{\pi^2} \frac{N_c^2 - 1}{\rho \min(L, L_c)} \frac{y}{\sqrt{2\xi_s y}}. \quad (59)$$

At scales $q_T^2 < Q_s^2$, Eq. (55) is no longer valid since saturation effects take place which tame the growth of the gluon distribution function. Inspired by the KLN model of saturation [35], we use a simplified model for the unintegrated gluon distribution function

$$\phi(x, q_T^2) = \begin{cases} \frac{2}{\pi^2} \frac{N_c^2 - 1}{\rho \min(L, L_c)} \frac{y}{\sqrt{2\xi_s y}}, & q_T^2 < Q_s^2; \\ \phi_{DLA}(x, q_T^2), & q_T^2 > Q_s^2. \end{cases} \quad (60)$$

We can then express \hat{q}_R in Eq. (14) as

$$\begin{aligned} \hat{q}_R &= \frac{C_R}{N_c} \frac{4\pi^2 \rho}{N_c^2 - 1} \int dx \left[\int_0^{Q_s^2} \frac{d^2 q_T}{(2\pi)^2} \delta(x - \frac{q_T^2}{Q_{max}^2}) \right. \\ &\quad \times \alpha_s(q_T^2) N_c \phi_{DLA}(x, Q_s^2) + \int_{Q_s^2}^{Q_{max}^2} \frac{d^2 q_T}{(2\pi)^2} \\ &\quad \left. \times \delta(x - \frac{q_T^2}{Q_{max}^2}) \alpha_s(q_T^2) N_c \phi_{DLA}(x, q_T^2) \right], \end{aligned} \quad (61)$$

where $Q_{max}^2 \approx 6ET$. Integrating out the δ -function, we have

$$\begin{aligned} \hat{q}_R &= \frac{C_R}{N_c} \frac{2}{\pi} Q_{max}^2 \int_0^{x_m} dx \frac{\alpha_s(x Q_{max}^2) N_c}{\min(L, L_c)} \\ &\quad \times \frac{\ln \frac{1}{x}}{\sqrt{2 \ln \frac{1}{x} \xi(x Q_{max}^2)}} + \frac{C_R}{N_c} \frac{4\pi^2 \rho}{N_c^2 - 1} \\ &\quad \times \int_{x_m}^1 dx N_c \alpha_s(x Q_{max}^2) \phi_{DLA}(x, x Q_{max}^2), \end{aligned} \quad (62)$$

where $x_m = Q_s^2/Q_{max}^2$.

VI. CONFORMAL PLASMA

We first examine the behavior of the saturation scale and jet transport parameter in a medium with fixed coupling constant. For a medium length L that is always larger than the coherence length for any jet energy, we find

$$\ln \frac{Q_s^2}{\mu^2} \sim \ln \frac{1}{x}, \quad (63)$$

for small x . This means that both constraints in Eqs. (50) and (51) are fulfilled at small coupling $\bar{\lambda}$. We can then use the DLA approximation to describe the evolution of the gluon distribution function and evaluate the saturation scale and transport parameter at small $x_m \sim 1/E$. Note that the eikonal approximation is valid for distances such that the total momentum transferred to the probe $\hat{q}L \ll Q_{max}^2$, since Q_{max}^2 is the momentum transfer for a large angle (90°) scattering. From this requirement and Eq. (67) we find

$$\bar{\lambda}L \ll L_c \frac{Q_{max}^2}{Q_s^2}, \quad (64)$$

which is compatible with the weak coupling approximation and $L > L_c$ if $Q_{max}^2 \gg Q_s^2$.

We determine the saturation scale by solving the self-consistent equation Eq. (56). Treating B as a constant and using the definition of ξ for fixed coupling constant [Eq. (52)] at $Q_s^2(x_m)$ and $x_m = Q_s^2(x_m)/Q_{max}^2$, one obtains

$$\begin{aligned} \ln \frac{Q_s^2(x_m)}{\mu^2} &= \frac{1}{2} \left[\frac{2}{2 + \bar{\lambda}} \ln \frac{B}{T\mu^2} + \ln \frac{Q_{max}^2}{\mu^2} \right. \\ &\quad \left. + \sqrt{\frac{\bar{\lambda}}{2 + \bar{\lambda}} \ln^2 \frac{Q_{max}^2}{\mu^2} - \frac{2\bar{\lambda}}{(2 + \bar{\lambda})^2} \ln^2 \frac{B}{T\mu^2}} \right]. \end{aligned} \quad (65)$$

In the large energy limit, the above solution simplifies to

$$\frac{Q_s^2(x_m)}{\mu^2} \approx \left(\frac{B}{\mu^2 T}\right)^{\frac{1}{2+\bar{\lambda}}} \left(\frac{Q_{max}^2}{\mu^2}\right)^{\frac{1}{2} + \frac{1}{2}\sqrt{\frac{\bar{\lambda}}{2+\bar{\lambda}}}}. \quad (66)$$

To compute the quenching parameter we study numerically the integral in Eq. (62) and find that, for the infinite conformal plasma, it can be well approximated by

$$\begin{aligned} \hat{q}_R &= \frac{C_R}{N_c} \frac{Q_s^2(x_m)}{\min(L, L_c(x_m))} \frac{2}{\pi} \alpha_s(Q_s^2(x_m)) \\ &\times N_c \ln \frac{1}{x_m} \left[\frac{\delta_L}{\sqrt{2 \ln \frac{1}{x_m} \xi(Q_s^2(x_m))}} \right. \\ &\left. + \frac{1}{\xi(Q_s^2(x_m)) - \frac{2}{\pi} N_c \alpha_s(Q_s^2(x_m)) \ln \frac{1}{x_m}} \right]. \quad (67) \end{aligned}$$

This is a very good approximation for values of $\bar{\lambda} > 1$. For small $\bar{\lambda}$ it approximates the exact integral within a factor 2 as long as $\bar{\lambda} \ln(Q_{max}^2/T^2) > 1$. Substituting Eq. (66) in Eq. (67) we find

$$\begin{aligned} \hat{q}_R &= \frac{C_R}{N_c} Q_s^2(x_m) T x_m \left(\frac{\ln \frac{1}{x_m}}{\ln \frac{x_m^2 Q_{max}^2}{\mu^2}} \right. \\ &\left. + \frac{1}{2} \sqrt{\frac{\bar{\lambda}}{2}} \frac{\ln \frac{1}{x_m}}{\sqrt{\ln \frac{1}{x_m} \ln \frac{x_m Q_{max}^2}{\mu^2}}} \right). \quad (68) \end{aligned}$$

As expected [39], the transport parameter is determined by the saturation scale.

To determine the dependence on the coupling, we substitute the definition of B and set $\mu^2 = T^2$

$$\begin{aligned} \frac{\hat{q}_R}{T^3} &= \frac{C_R}{N_c} \left(\frac{Q_{max}^2}{T^2}\right)^{\sqrt{\frac{\bar{\lambda}}{2+\bar{\lambda}}}} \left[\frac{\pi^{5/2} \bar{\lambda}^{5/4} (2+\bar{\lambda})^{1/4}}{36 \sqrt{\ln Q_{max}^2/T^2}} \right]^{\frac{2}{2+\bar{\lambda}}} \\ &\times \left(\sqrt{2+\bar{\lambda}} - \sqrt{\bar{\lambda}} \right)^{\frac{4+\bar{\lambda}}{2+\bar{\lambda}}} \frac{1}{4} \left[\sqrt{\bar{\lambda}} + \frac{2}{\sqrt{\bar{\lambda}}} \right]. \quad (69) \end{aligned}$$

Let us point out two interesting features in the above result: 1) \hat{q}_R grows as a coupling dependent power of the energy and 2) it depends non analytically on the reduced t'Hooft coupling $\bar{\lambda}$. The non-analyticity is a consequence of the evolution process.

The derivation of Eq. (69) for a conformal plasma is strictly valid for small values of $\bar{\lambda}$ since both the evolution equation Eq. (47) and the initial conditions Eq. (31) are based on perturbation theory. However, in our computation we have not make any further assumption about the smallness of $\bar{\lambda}$. Given the recent interest in the computation of transport properties in strongly coupled $\mathcal{N} = 4$ SYM [21, 22, 23, 40, 41], it is still instructive to study the strong coupling behavior of the jet transport parameter. Plotted in Fig. 3 is the jet transport parameter as a function of the reduced t'Hooft coupling $\bar{\lambda}$, normalized by its large coupling limit,

$$\hat{q}_R(\bar{\lambda} = \infty) = \frac{C_R}{N_c} \frac{T Q_{max}^2}{4} = \frac{C_R}{N_c} \frac{3T^2 E}{2}. \quad (70)$$

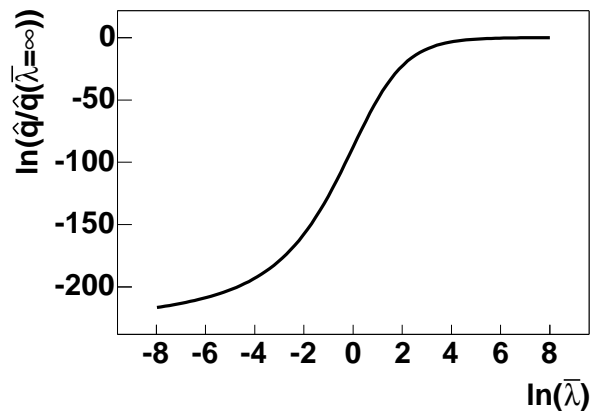


FIG. 3: Normalized jet transport parameter as a function of reduced t'Hooft coupling $\bar{\lambda}$ in a formal plasma for an energetic probe of $\log_{10}(Q_{max}^2/T^2) = 90$.

The normalized jet transport parameter increases monotonically with the coupling $\bar{\lambda}$ and reaches its asymptotic value in the strong coupling limit. Note also that the above limit assumes that the energy of the probe is large such that $\ln(Q_{max}^2/T^2) \gg \ln \bar{\lambda}$.

Several comments on this strong coupling limit are in order:

- In the strong coupling limit, the saturation scale approaches its maximum limit $Q_s^2(x_m) = Q_{max}^2$ and, thus, the eikonal approximation is questionable. Both the saturation scale and the transport parameter become independence of the initial condition as contained in B .
- Eq. (70) has a power dependence on the energy of the probe, and the power becomes coupling independent in the strong coupling limit.
- Contribution to Eq. (70) comes completely from the saturated part of the gluon distribution function. We have performed a simplified treatment of this region by considering it constant. This is well motivated by numerical solutions of the Balitsky-Kovchegov equations at weak coupling [42, 43]. However, at strong coupling extra dependencies on the coupling (subleading at weak coupling) may become important.
- We have not considered the evolution of the wave function of the probe. This is motivated by the weak coupling picture, in which such evolution is considered separately as the radiative processes of the probe and are described by radiative energy loss. At strong coupling this separation of the probe and medium evolution becomes ambiguous and may lead to an extra coupling dependence.

VII. NON-CONFORMAL PLASMA

From the analysis of a conformal plasma with a fixed coupling we concluded that the saturation scale grows faster than any logarithmic jet energy dependence. Since the typical momentum scale is dictated by Q_s^2 , effects of a running coupling constant become important in the QCD plasma for large energy probes. This issue is addressed by solving numerically Eq. (62) with ξ given by Eq. (52). In this case we find that Eq. (62) is well approximated (within 20 %) ³ by

$$\hat{q}_R = \frac{C_R}{N_c} \frac{Q_s^2}{\min(L, L_c)} \frac{\ln \frac{1}{x_m}}{\ln \frac{Q_s^2(x_m)}{\Lambda^2}} \times \left[\frac{\delta_L}{\sqrt{\pi \frac{b}{N_c} \ln \frac{1}{x_m} \ln \left(\ln \frac{Q_s^2}{\Lambda^2} / \ln \frac{\mu^2}{\Lambda^2} \right)}} + \frac{1}{\ln \left(\ln \frac{Q_s^2}{\Lambda^2} / \ln \frac{\mu^2}{\Lambda^2} \right) - \frac{\ln(1/x_m)}{\ln(Q_s^2(x_m)/\Lambda^2)}} \right], \quad (71)$$

where $\delta_L = 1/2$ if $L > L_c$ and $\delta_L = 1$ otherwise. As in the conformal case, \hat{q}_R is determined by the saturation scale, which is given by

$$Q_s^2 = B(x, Q_s^2) \min(L, L_c) \times e^{\sqrt{\frac{4N_c}{\pi b} \ln \left(\ln \frac{Q_s^2}{\Lambda^2} / \ln \frac{\mu^2}{\Lambda^2} \right) \ln \frac{1}{x_m}}}, \quad (72)$$

where $B(x, Q_s^2)$ is given in Eq. (57) and $L_c = 1/x_m T = Q_s^2(x_m)/Q_{max}^2 T$.

As in the conformal case, the saturation scale and jet transport parameter have a fast growth with the jet energy. In spite of the fact that the above results are derived with an approximation for asymptotically small x (which implies large saturation scales), we would like to make some numerical evaluations of the jet transport parameter for jet energies accessible at RHIC and LHC and address the experimental consequences of this growth.

We solve numerically the self-consistent equation Eq. (72) for the saturation scale $Q_s^2(x_m)$. In order to avoid the infrared singularity of α_s we regulate the coupling constant as

$$\alpha_s(Q^2) = \frac{1}{b} \frac{1}{\ln \frac{Q^2 + T^2}{\Lambda^2}}. \quad (73)$$

To be consistent, we also replace

$$\ln \left(\ln \frac{Q_s^2}{\Lambda^2} / \ln \frac{\mu^2}{\Lambda^2} \right) \rightarrow \ln \left(\ln \frac{Q_s^2 + T^2}{\Lambda^2} / \ln \frac{\mu^2 + T^2}{\Lambda^2} \right).$$

³ For determining this expression we assumed that the coherence length is always larger or smaller than the path length. In the numerical computations presented this is not assumed and the $\min()$ is replaced by a smooth function.

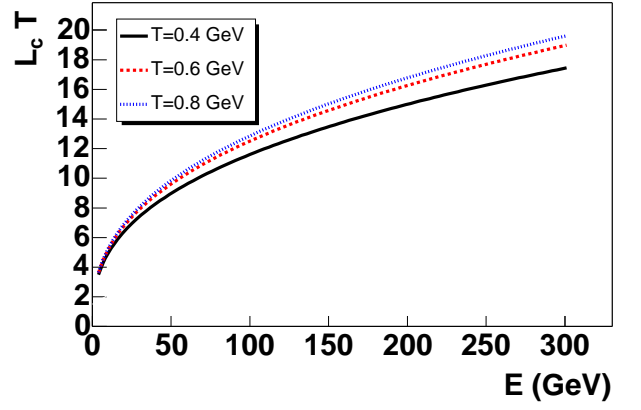


FIG. 4: (Color online) Coherence length times temperature as a function of the energy of the probe for different temperatures.

The coupling constant at a thermal scale is determined by solving the coupled equations,

$$\alpha_s^T = \frac{1}{b} \frac{1}{\ln \frac{Q_s^2(T) + T^2}{\Lambda^2}}, \quad (74)$$

$$Q_s^2(T) = 18\pi \frac{(N_c \alpha_s^T)^2}{Q_s^2(T)} T^4, \quad (75)$$

which are essentially Eq. (37) at $x = Q_s^2(T)/18T^2$ [we have set the logarithms in Eq. (37) to be of order 1]. Finally, since Eq. (72) is only valid for asymptotically large rapidities y , we also shift the rapidities to

$$y \rightarrow y + y_0, \quad (76)$$

with $y_0 = 0.24$. This value has been chosen such that as y decreases we recover the value of the saturation scale $Q_s^2(T)$. In the following numerical evaluation we will choose $\mu^2 = T^2$ and $\Lambda = 200$ MeV.

Since the medium is finite in heavy ion collisions, we start by studying the coherence length. This is computed by solving

$$L_c^2 \equiv \frac{1}{x_m^2 T^2} = \frac{6E}{B} e^{-\sqrt{\frac{4N_c}{\pi b} \ln \left(\ln \frac{Q_s^2(x_m)}{\Lambda^2} / \ln \frac{\mu^2}{\Lambda^2} \right) \ln \frac{1}{x_m}}}. \quad (77)$$

This coherent length is used to calculate the saturation scale for any large medium size $L > L_c$. For small medium size, $L < L_c$, the actual length L is used to calculate the saturation scale. The coherence length is plotted in Fig. 4 and it shows a strong energy dependence, as can be inferred from Eq. (77). This strong jet energy dependence $L_c \sim \sqrt{E}$ is approximately independent of the evolution of the gluon distribution function, and stems from the definition of the coherence length as $L_c = 1/xT$. As expected from the running coupling, it does not scale with temperature. For a characteristic

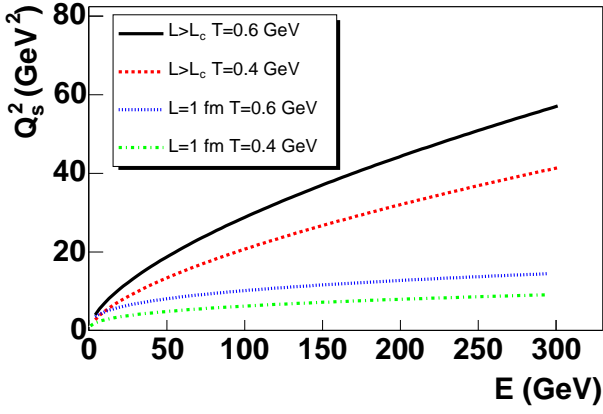


FIG. 5: (Color online) Saturation scale as a function of the jet energy.

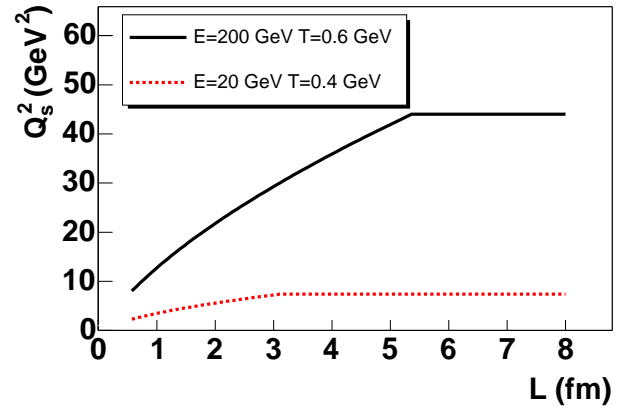


FIG. 7: (Color online) Saturation scale as a function of the path length for different probe energies.

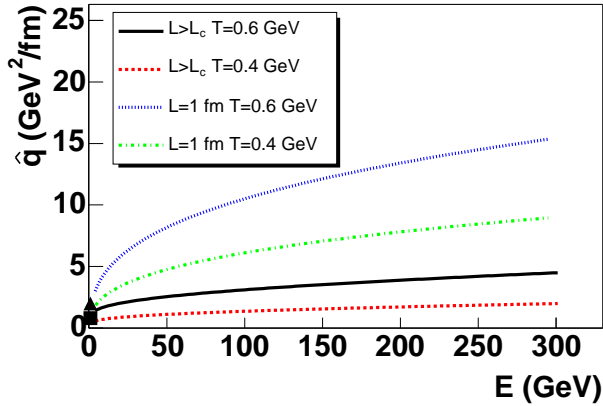


FIG. 6: (Color online) Jet quenching parameter \hat{q} as a function of the jet energy. The square (triangle) marks the value of \hat{q} for thermal particle at $T = 0.4$ GeV ($T = 0.6$ GeV). Significant corrections to the energy dependence are expected at low energy which should approach their thermal value at $E = 3T$.

temperature of $T = 0.4$ GeV in relativistic heavy ion collisions, the coherence length is significant: for a probe of $E = 20$ GeV, $L_c \approx 2.5$ fm while at $E = 100$ GeV, $L_c \approx 4.5$ fm, which are comparable with the nuclear size.

When the coherence length becomes comparable to the medium size a non-trivial length dependence of the saturation scale will arise, since the definition of Q_s^2 is different for path lengths longer or shorter than the coherence length. This is illustrated in Fig. 5 where the saturation scale is plotted as a function of the energy of the probe. When the path length is longer than the coherence length, Q_s^2 shows a stronger dependence on the energy. This is, in fact, driven by the energy dependence of the coherence length, and is mostly independent of the evolution of the medium gluon distribution. When the path length is smaller than the coherence length we obtain a significant reduction of the saturation

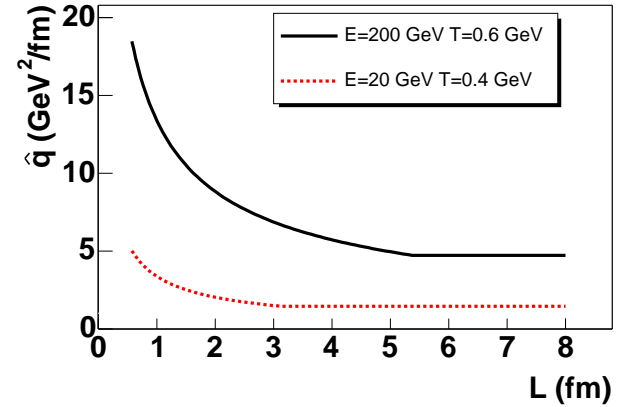


FIG. 8: (Color online) Jet quenching parameter \hat{q} as a function of the path length for different probe energies.

scale and a much weaker dependence on the energy, since the DLA evolution leads to a growth that is weaker than a power but faster than a logarithmic dependence. We note that the gluon saturation scale obtained here for a gluonic plasma is significantly larger than that in a nucleon, where $Q_s^2 \approx 1$ GeV² at $x \approx 10^{-4}$ [44]. This is a consequence of the fact that the QGP is a much denser system than a nucleon or cold nucleus. The saturation scale in a heavy nucleus is enhanced by a factor of $A^{1/3}$ and therefore might be large enough to facilitate a perturbative calculation of gluon distributions [45]. However, it is still an order of magnitude smaller than in a high temperature quark-gluon plasma.

In Fig. 6 we show the value of the jet quenching parameter \hat{q}_R from the integration of Eq. (62). For long path lengths \hat{q} becomes path length independent. The leading energy dependencies of both Q_s^2 and L_c cancel and the observed energy dependence is a consequence of the evolution of the medium gluon distribution. At shorter path lengths, we obtain an enhancement of \hat{q}_R as a consequence of the evolution.

The length dependence of both the saturation scale and the transport parameter is shown in Figs. 7 and 8 for different energies of the probe. As shown in Fig. 7, the saturation scale grows as a function of the path length. However this growth is smaller than linear. Thus, the transport parameter, as shown in Fig. 8, diverges at small path length. Note, however, that at very short path lengths ($L \ll \lambda_f$) the mean momentum broadening should vanish, since the probe has no medium to scatter with. Thus, we expect correction to the small L dependence of both Q_s^2 and \hat{q}_R . Finally, when the path length is larger than the coherence length both quantities become length independent. Note that we have assumed a simplified transition from the region $L < L_c$ to $L > L_c$. This is the reason for the abrupt change in the length dependence at $L = L_c$ in Figs. 7 and 8.

Let us remark that for path lengths smaller than the coherence length, the interaction of the probe with the whole length of the medium is coherent. Thus, if the length scales of space and time variation are smaller or comparable to the path length, the analysis of the saturation scales and jet transport parameter should be revisited. This will complicate the phenomenological extraction of the transport parameter in an expanding medium with strong spatial variation as in semi-peripheral heavy-ion collisions.

Because of the running of the coupling constant or the intrinsic scale (Λ) in QCD as a non-conformal gauge theory, the transport parameter \hat{q}_R has a non-trivial temperature dependence. To illustrate this, we plot in Fig. 9 the value of \hat{q}_R scaled by the energy density,

$$\epsilon = \frac{8\pi^2}{15} T^4, \quad (78)$$

to the power of 3/4 for the long path lengths ($L > L_c$). The dependence on the temperature is quite strong in the temperature range showed. This is not surprising since these temperatures are of the order of Λ and the coupling constant is very sensitive to the scale. The dependence, however, becomes weaker at higher temperatures. The jet energy dependence of the transport parameter is also stronger at lower temperatures. This, of course, is only a lower limit, since \hat{q}_R is larger for shorter path lengths⁴.

VIII. BOUND ON \hat{q} AND SHEAR VISCOSITY TO ENTROPY DENSITY RATIO

Following Ref. [20], one can relate the jet quenching parameter \hat{q}_R to the transport mean-free-path of the hard

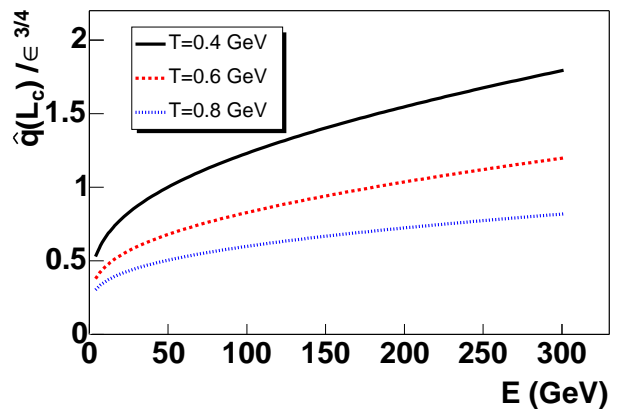


FIG. 9: (Color online) Jet quenching parameter scaled by $\epsilon^{3/4}$, with ϵ the energy density.

probe,

$$\lambda_f^{-1} \approx \frac{4\rho}{\langle \hat{s} \rangle} \int dq_T^2 q_T^2 \frac{d\sigma_R}{dq_T^2} = \frac{4\hat{q}_R(E)}{\langle \hat{s} \rangle}, \quad (79)$$

where we have used the definition of jet transport parameter in Eq. (2) and $\langle \hat{s} \rangle = Q_{max}^2 \approx 6ET$ is the average center-of-mass energy squared of the jet-gluon scattering. The requirement that the mean-free-path of the hard probe must be larger than the de Broglie wave length $1/E$ will set an upper bound for the energy loss parameter,

$$\hat{q}_R(E) \leq \frac{\langle \hat{s} \rangle E}{4} = \frac{3E^2 T}{2C}, \quad (80)$$

where C is a constant on the order of $\mathcal{O}(1)$.

We have checked that our numerical solutions of \hat{q}_R indeed satisfy this condition as shown in Fig. 10. For a conformal plasma, \hat{q}_R in Eq. (69) increases monotonically with the reduced t'Hooft coupling $\bar{\lambda}$ (see Fig. 3). In the limit $\bar{\lambda} \rightarrow \infty$, $Q_s^2(x_m) = Q_{max}^2$ and the jet transport parameter $\hat{q}_R = C_R T Q_{max}^2 / 4N_c$ for a gluon jet satisfies the bound for $E \geq T$. Since the strong coupling limit is an asymptotic behavior, the above bound on the transport parameter is also satisfied in the weak coupling limit of a conformal plasma.

For thermal partons with $\langle E \rangle \sim 3T$, the upper bound in Eq. (80) becomes

$$\frac{T^3}{\hat{q}_R(T)} \geq \frac{2}{27C}. \quad (81)$$

According to Ref. [20], one can also relate the shear viscosity to the transport parameter for a thermal parton,

$$\eta \approx \frac{1}{3} s T \lambda_f \approx s \frac{3T^3}{2\hat{q}_R(T)}, \quad \text{or} \quad \frac{\eta}{s} \approx \frac{3}{2} \frac{T^3}{\hat{q}_R(T)}. \quad (82)$$

Therefore, the upper bound on the transport parameter $\hat{q}_R(T)$ also provides a lower bound on the shear viscosity

⁴ The initial value of \hat{q}_R before evolution is about half that of [46]. The main reason is that we use $\alpha_s = 0.3$ for $T = 0.4$ GeV while in [46], $\alpha_s = 0.5$.

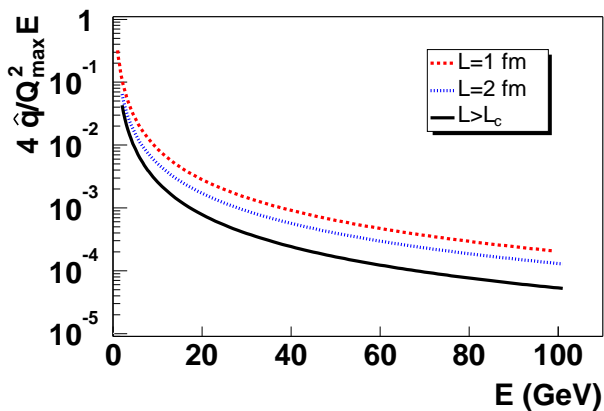


FIG. 10: (Color online) Ratio $4\hat{q}/Q_{max}^2 E = 2\hat{q}/3E^2 T$ as a function of jet energy E .

to entropy density ratio

$$\frac{\eta}{s} \geq \frac{1}{9C}. \quad (83)$$

This is very similar to the bound found by Danielewicz and Gyulassy [47] from transport theory and the bound $1/4\pi$ found in the strong coupling limit of $\mathcal{N} = 4$ SYM [48].

The upper bound on the transport parameter \hat{q}_R in Eq. (80) and its connection with the shear viscosity in Eq. (82) are quite general since they do not rely on any assumption about the nature (perturbative or nonperturbative) of parton interaction inside the medium. They do rely, however, on a transport description of the plasma in terms of quasi-particles. Therefore, it is not surprising that the connection between the transport parameter and shear viscosity does not hold in the strong coupling limit of $\mathcal{N} = 4$ SYM theory, since thermal modes in such a strongly coupled theory cannot be described as quasi-particles [49].

We should emphasize that the jet transport parameter is an intrinsic property of the medium which could be dominated by non-perturbative physics. However, in the case of large saturation scale Q_s^2 and transverse momentum transfer, the evolution of the gluon distribution function and the jet transport parameter should still be described by perturbative QCD and so should the interaction between jet and the medium and the radiative energy loss. Therefore, as far as the transport description of the dense medium is valid, one can use the energy dependence of the jet (parton) transport parameter $\hat{q}_R(E)$ as determined by jet quenching phenomenology to estimate the shear viscosity to entropy density ratio via extrapolation.

With a recent phenomenological study of both single and dihadron spectra suppression using the next-to-leading order (NLO) pQCD parton model calculation [13], the average gluon jet energy loss per unit length in

a 1-d expanding medium is estimated to be

$$\left(\frac{dE}{dL}\right)_{1d} \approx 1.9 - 3.4 \text{ GeV/fm}, \quad (84)$$

for $E = 10 - 15$ GeV, which also includes an empirical variation with jet energy. Using the relationship between parton energy loss and the transport parameter in Eq. (1), one obtains an estimate of the average gluon jet transport parameter

$$\hat{q}_0(E) = \frac{2}{\tau_0 \alpha_s N_c} \left(\frac{dE}{dL}\right)_{1d} \approx 1.0 - 1.9 \text{ GeV}^2/\text{fm} \quad (85)$$

at an initial time $\tau_0 = 1 \text{ fm}/c$ ⁵. Here, we used $\alpha_s \approx 0.24$ at $Q_s^2 \approx 5 \text{ GeV}^2$ in a pure gluonic plasma. This roughly agrees with the numerical calculation in Fig. 8. As shown in Fig. 6, the energy dependence of \hat{q}_R is very weak for $E < 20$ GeV and long propagation length. Even for short propagation length $L \sim L_c \sim 2$ fm, the energy dependence is limited to about 25% variation. We therefore can use the above estimate for thermal parton transport parameter. Using the same initial temperature $T_0 = (337 \pm 10) \text{ MeV}$ as in Ref. [20], one obtains

$$\frac{\eta_0}{s_0} \approx \frac{3}{2} \frac{T_0^3}{\hat{q}_0(T)} \approx 0.15 - 0.24. \quad (86)$$

For more consistent analysis, one should consider explicit energy dependence of the parton energy loss beyond that in \hat{q}_R .

Finally, the requirement that the coherence length is larger than the mean-free-path of thermal particle sets a limit on the coupling constant α_s^T . Indeed, from Eq. (79) and Eq. (71) $\hat{q}_R \approx x_m Q_s^2(x_m) T$, we find

$$x_m = Q_s(x_m) / \langle \hat{s} \rangle \leq 1/4. \quad (87)$$

This bound is only satisfied at weak coupling

$$2N_c \alpha_s^T \sqrt{2\pi \ln \frac{1}{N_c g^2}} \leq 1. \quad (88)$$

For larger values of the coupling α_s^T , coherence effects in the multiple scattering of thermal particles become important.

IX. SUMMARY AND DISCUSSIONS

In this paper we have studied the energy dependence of the jet transport (or quenching) parameter \hat{q}_R . By relating \hat{q}_R to the unintegrated gluon distribution function

⁵ This phenomenological analysis was based on the assumption that \hat{q} is independent of the path length. The nontrivial length dependence of \hat{q} as obtained in this paper will affect the extracted average value of the jet transport parameter.

of the plasma we have shown that the energy dependence of \hat{q}_R arises from the evolution of the gluon distribution function. Thermal quarks and gluons in the plasma play the same role as the valence quarks of the nucleus and high energy jets probe their wave functions at small x . Similar as in a cold nuclear matter, the evolution leads to a growth in the gluon number which is eventually tamed by saturation effects. Therefore, the jet transport parameter, also defined as the momentum broadening per unit length, is determined by the saturation scale Q_s^2 .

Using thermal field theory with HTL resummation, we have derived the gluon distribution function for scales $\mu^2 < T^2$ as probed by the interactions among thermal partons. For such interaction among thermal partons, the coherence length is smaller than the mean-free-path and, thus, the saturation scale grows fast for small x , $Q_s^2 \sim 1/x$. Remarkably, evaluating the saturation scale at the typical x of the scattering among thermal partons, $x \approx Q_s^2/4T^2$, leads to $Q_s^2 \sim \mu_D^2$. Therefore, the typical momentum transfer is of the order of μ_D as expected. What is more interesting is that, for large angle scattering of thermal particles with $x \sim 1$, the saturation scales is of the order of the magnetic mass $Q_s^2 \sim \mu_{mag}^2$.

The hard thermal loop result for gluon distribution function serves as the initial condition of the evolution of the gluon distribution as probed by an energetic jet. Since this process involves scales much larger than the medium scale, we have neglected thermal modification of the evolution kernel. We then used the double logarithmic approximation to describe the evolution in a conformal theory and in (pure glue) QCD.

For a conformal plasma, both the saturation scale and the jet transport parameter \hat{q}_R grow with energy as a coupling-dependent power. The evolution leads to a \hat{q}_R which is non-analytic in the t'Hooft coupling $\lambda = g^2 N_c$. In the large coupling limit, \hat{q}_R becomes independent of the coupling and grows linearly with E . This is very different from results obtained in $\mathcal{N} = 4$ SYM [21, 22, 23, 40, 41]. As remarkable as this may be, the analysis we have performed is perturbative in nature and the extrapolation to infinite coupling might not be justified.

In the case of (pure glue) QCD, the evolution leads to a jet energy dependence of the transport parameter that is stronger than any power of logarithmic dependence. The saturation effect also gives rise to a non-trivial length dependence of the jet transport parameter. The running of coupling constant also results in a significant temperature dependence which becomes weaker at higher temperatures. We have numerically evaluated the saturation scale and jet transport parameter in a temperature range $T = 0.4 - 0.6$ GeV that is relevant for relativistic heavy ion collisions at RHIC and LHC. The growth of \hat{q}_R with jet energy is modest for large medium size $L \gg L_c$. However, the energy dependence is significant for $L \lesssim L_c$. The obtained transport parameter is also larger than that computed via perturbation theory without evolution [46]. For $T = 0.4$ GeV and $E = 10 - 20$ GeV, our

computed value $\hat{q}_R \approx 1.5 - 2$ GeV²/fm for a gluon jet is in agreement with the results from recent phenomenological studies of experimental data on jet quenching at RHIC [11, 12, 13, 50]. It is, however, smaller than the results from phenomenological studies [10, 51] based on an implementation of energy loss by Salgado and Wiedemann (SW) [52]. A recent study within this model with explicit space-time dependent profiles of energy density from 2 and 3-D hydro calculations gives a transverse averaged $\hat{q}_R \approx 4 - 5$ GeV²/fm [53] at initial time $\tau_0 = 1$ fm/c. Inclusion of dihadron suppression in the phenomenological study has been shown [13] to greatly improve the sensitivity of jet quenching to variation of \hat{q}_R . It is clear that inclusion of the energy and length dependence of the jet transport parameter will also influence the phenomenological study of the jet quenching measurements.

Given the relation between shear viscosity η and transport parameter $\hat{q}_R(T)$ for a thermal parton as derived recently in Ref. [20], the energy dependence of jet transport parameter determined from theoretical and phenomenological studies can also be used to estimate the shear viscosity in the dense matter produced in heavy-ion collisions. This will unify high p_T and low p_T aspects of heavy-ion collisions. The latter can characterize the collective behavior of the produced dense matter which is well described by relativistic hydrodynamics with a negligible shear viscosity [54]. We have also derived an upper bound on the transport parameter of high energy jets. This upper bound can lead to a lower bound on the shear viscosity to entropy density ratio which is consistent with other transport studies.

The saturation scale in a glue plasma we obtained in this study is much larger than that in a cold nucleus or a nucleon at extremely small x . This results from the high gluon density in a plasma with coherence length comparable to the medium size. This is quite different from the analysis of Hadron-Electron Ring Accelerator (HERA) data which leads to a power dependence of Q_s^2 on x [44]

$$Q_s^2 = 1 \text{ GeV} \left(\frac{3 \times 10^{-4}}{x} \right)^{0.288}, \quad (89)$$

where the coherence length is much larger than the nucleon size. When the coherence length is comparable to the medium length, the saturation scale is not linear with the path length. Thus, instead of using the phenomenological expression Eq. (89), we used the DLA approximation to estimate Q_s^2 . Numerical solutions to the Balitsky-Kovchegov (BK) equation with running coupling constant [42, 43] show that the unintegrated gluon distribution is consistent with the DLA asymptotes and that the saturation scale behaves as $Q_s^2 \sim \exp\{\Delta\sqrt{y}\}$, similar to what is expected from the DLA asymptotes. Note, however, that these conclusions are for large values of the rapidity, $y \sim 10$, while in our case the typical x probed by high energy jets in the kinematic range relevant to heavy-ion collisions at RHIC and LHC is not very small, $x \sim 0.1$. The large values of x obtained imply that

significant corrections to the obtained behavior may occur, which could be addressed by a numerical analysis of the BK equation.

Acknowledgments: This work was supported in part

by the U. S. Department of Energy under grant contract DE-AC02-05CH11231. We thank J. L. Albacete, N. Armesto, P. Jacobs, C. Salgado, D. Teaney, T. Renk and U. Wiedemann for fruitful discussions.

-
- [1] K. Adcox *et al.*, [PHENIX Collaboration], Phys. Rev. Lett. **88**, 022301 (2002).
- [2] C. Adler *et al.*, [STAR Collaboration], Phys. Rev. Lett. **89** 202301 (2002).
- [3] C. Adler *et al.*, [STAR Collaboration], Phys. Rev. Lett. **90**, 082302 (2003).
- [4] M. Gyulassy, I. Vitev, X. N. Wang and B. W. Zhang, arXiv:nucl-th/0302077.
- [5] X.-N. Wang, Nucl. Phys. A **750**, 98 (2005).
- [6] For a recent review on experimental and phenomenological studies, see P. Jacobs and X. N. Wang, Prog. Part. Nucl. Phys. **54**, 443 (2005).
- [7] R. Baier, Y. L. Dokshitzer, A. H. Mueller, S. Peigne and D. Schiff, Nucl. Phys. B **484**, 265 (1997).
- [8] I. Vitev and M. Gyulassy, Phys. Rev. Lett. **89**, 252301 (2002).
- [9] X.-N. Wang, Phys. Lett. B **595**, 165 (2004).
- [10] K. J. Eskola, H. Honkanen, C. A. Salgado and U. A. Wiedemann, Nucl. Phys. A **747**, 511 (2005).
- [11] S. Turbide, C. Gale, S. Jeon and G. D. Moore, Phys. Rev. C **72**, 014906 (2005) [arXiv:hep-ph/0502248].
- [12] For a comparison of different models and their phenomenology, see A. Majumder, J. Phys. G **34**, S377 (2007) [arXiv:nucl-th/0702066].
- [13] H. Zhang, J. F. Owens, E. Wang and X. N. Wang, Phys. Rev. Lett. **98**, 212301 (2007) [arXiv:nucl-th/0701045].
- [14] E. Wang and X.-N. Wang, Phys. Rev. Lett. **89**, 162301 (2002).
- [15] M. Gyulassy and X.-N. Wang, Nucl. Phys. B **420**, 583 (1994).
- [16] B. G. Zakharov, JETP Lett. **63**, 952 (1996).
- [17] U. Wiedemann, Nucl. Phys. **B588**, 303 (2000).
- [18] M. Gyulassy, P. Lévai and I. Vitev, Nucl. Phys. **B594**, 371 (2001).
- [19] X. F. Guo and X.-N. Wang, Phys. Rev. Lett. **85**, 3591 (2000); Nucl. Phys. A **696**, 788 (2001).
- [20] A. Majumder, B. Muller and X. N. Wang, Phys. Rev. Lett. **99**, 192301 (2007).
- [21] H. Liu, K. Rajagopal and U. A. Wiedemann, Phys. Rev. Lett. **97**, 182301 (2006); arXiv:hep-ph/0612168.
- [22] S. S. Gubser, Nucl. Phys. B **790**, 175 (2008) [arXiv:hep-th/0612143].
- [23] J. Casalderrey-Solana and D. Teaney, JHEP **0704**, 039 (2007) [arXiv:hep-th/0701123].
J. Casalderrey-Solana and D. Teaney, arXiv:hep-th/0701123.
- [24] M. Luo, J. W. Qiu and G. Sterman, Phys. Lett. B **279** (1992) 377; Phys. Rev. D **50** (1994) 1951; Phys. Rev. D **49**, 4493 (1994).
- [25] X. N. Wang, Phys. Lett. B **650**, 213 (2007).
- [26] X. F. Guo, Phys. Rev. D **58**, 114033 (1998).
- [27] A. Majumder and B. Muller, arXiv:0705.1147 [nucl-th].
- [28] T. S. Biro and B. Muller, Nucl. Phys. A **561** (1993) 477.
- [29] G. Alexanian and V. P. Nair, Phys. Lett. B **352**, 435 (1995).
- [30] G. M. von Hippel and R. R. Horgan, Phys. Rev. Lett. **90**, 132001 (2003).
- [31] R. D. Pisarski, Phys. Rev. Lett. **63**, 1129 (1989).
- [32] H. A. Weldon, Phys. Rev. D **26**, 1394 (1982); Phys. Rev. D **28**, 2007 (1983).
- [33] A. H. Mueller, Nucl. Phys. B **558**, 285 (1999).
- [34] X. N. Wang, Phys. Lett. B **485**, 157 (2000).
- [35] D. Kharzeev and M. Nardi, Phys. Lett. B **507**, 121 (2001). D. Kharzeev and E. Levin, Phys. Lett. B **523**, 79 (2001). D. Kharzeev, E. Levin and M. Nardi, Nucl. Phys. A **730**, 448 (2004) [Erratum-ibid. A **743**, 329 (2004)].
- [36] L. V. Gribov, E. M. Levin and M. G. Ryskin, Nucl. Phys. B **188**, 555 (1981).
- [37] A. H. Mueller and J. W. Qiu, Nucl. Phys. B **268**, 427 (1986).
- [38] Y. L. Dokshitzer, Sov. Phys. JETP **46**, 641 (1977) [Zh. Eksp. Teor. Fiz. **73**, 1216 (1977)].
- [39] R. Baier, Nucl. Phys. A **715**, 209 (2003).
- [40] C. P. Herzog, A. Karch, P. Kovtun, C. Kozcaz and L. G. Yaffe, JHEP **0607**, 013 (2006).
- [41] J. Casalderrey-Solana and D. Teaney, Phys. Rev. D **74**, 085012 (2006).
- [42] J. L. Albacete, N. Armesto, J. G. Milhano, C. A. Salgado and U. A. Wiedemann, Phys. Rev. D **71**, 014003 (2005).
- [43] J. L. Albacete and Y. V. Kovchegov, Phys. Rev. D **75**, 125021 (2007) [arXiv:0704.0612 [hep-ph]].
- [44] K. Golec-Biernat and M. Wusthoff, Phys. Rev. D **59**, 014017 (1999).
- [45] L. D. McLerran and R. Venugopalan, Phys. Rev. D **49**, 2233 (1994).
- [46] R. Baier and D. Schiff, JHEP **0609**, 059 (2006).
- [47] P. Danielewicz and M. Gyulassy, Phys. Rev. D **31**, 53 (1985).
- [48] G. Policastro, D. T. Son and A. O. Starinets, Phys. Rev. Lett. **87**, 081601 (2001).
- [49] D. Teaney, Phys. Rev. D **74**, 045025 (2006).
- [50] A. Majumder, C. Nonaka and S. A. Bass, Phys. Rev. C **76**, 041902 (2007) [arXiv:nucl-th/0703019].
- [51] A. Dainese, C. Loizides and G. Paic, Eur. Phys. J. C **38**, 461 (2005).
- [52] C. A. Salgado and U. A. Wiedemann, Phys. Rev. D **68**, 014008 (2003).
- [53] T. Renk and K. Eskola, Phys. Rev. C **75**, 054910 (2007) [arXiv:hep-ph/0610059]; T. Renk, private communication.
- [54] D. Teaney, Phys. Rev. C **68**, 034913 (2003).